Improved representation of the diurnal variation of warm season precipitation by an atmospheric general circulation model at a 10 km horizontal resolution

Hyerim Kim[1] · Myong-In Lee[1] · Dong-Hyun Cha[1] · Young-Kwon Lim[2,3] · William M. Putman[2]

Abstract

This study investigates the diurnal variation of the warm season precipitation simulated by the Goddard Earth Observing System version 5 atmospheric general circulation model for 2 years (2005–2006) at a horizontal resolution of 10 km. The simulation was validated with the satellite-derived Tropical Rainfall Measuring Mission (TRMM) 3B42 precipitation data and the Modern-Era Retrospective analysis for Research and Applications atmospheric reanalysis for atmospheric winds and moisture. The simulation is compared with the coarse-resolution run in 50 km to examine the impacts driven by resolution change. Overall, the 10 km model tends to reproduce the important features of the observed diurnal variation, such as the amplitude and phase at which precipitation peaks in the evening on land and in the morning over the ocean, despite an excessive amplitude bias over land. The model also reproduces the realistic propagation patterns of precipitation in the vicinity of ocean coasts and major mountains. The regional characteristics of the diurnal precipitation over two regions, the Bay of Bengal and the Great Plains in North America, are examined in detail, where the observed diurnal cycle exhibits a systematic transition in the peak phase due to the development and propagation of regional-scale convective systems. The model is able to reproduce this pattern as well as the diurnal variation of low-level wind and moisture convergence; however, it is less effective at representing the nocturnal peak of precipitation over the Great Plains. The model results suggest that increasing the horizontal resolution of the model to 10 km substantially improves the representation of the diurnal precipitation cycle. However, intrinsic model deficiencies in topographical precipitation and the accurate representation of mesoscale convective systems remain a challenge.

Keywords Diurnal variation · Precipitation · General circulation model · Horizontal resolution

1 Introduction

Diurnal variation of precipitation is a fundamental component of the global climate system, especially in warm seasons. Previous studies analyzing observation data have demonstrated that there are large differences in the diurnal variation between the continent and the ocean continental and oceanic environments, such that the continental deep convection produces precipitation more frequently in the late afternoon to evening, whereas the oceanic precipitation develops more typically during the early morning (Yang and Slingo 2001; Dai et al. 2007; Kikuchi and Wang 2008). They also indicate that the diurnal (24-h) component has a greater influence than the semidiurnal (12-h) component both on land and on the ocean. Kikuchi and Wang (2008) demonstrated that the first and second modes of an empirical orthogonal function (EOF) analysis representing the 24-h

✉ Myong-In Lee
  milee@unist.ac.kr

1   School of Urban and Environmental Engineering, Ulsan National Institute of Science and Technology, Ulsan, South Korea

2   Global Modeling and Assimilation Office, NASA Goddard Space Flight Center, Greenbelt, MD, USA

3   Goddard Earth Science, Technology, and Research/I.M. Systems Group, Greenbelt, MD, USA

cycle accounted for more than 80% of the total rainfall variability, based on 3-h interval Tropical Rainfall Measuring Mission (TRMM) precipitation data. In contrast, the third and fourth modes representing the 12-h cycle accounted for less than 10% of the total variability.

Although the ultimate source of the variation is the difference in radiation between day and night, the diurnal cycle of warm-season precipitation has a distinctive geographical variation in terms of the amplitude and peak phase, being affected complicatedly by local and large-scale dynamical and thermal processes (Yang and Slingo 2001; Sorooshian et al. 2002; Lee et al. 2007c; Yuan et al. 2013). The organization and propagation of weather systems result in differences in the amplitude and the peak phase. For example, diurnal precipitation over coastal regions exhibits a systematic change in amplitude and phase along its propagation path toward the open ocean. A wide range of diurnal variation is observed over the island of Sumatra in the Maritime Continent (i.e., a region in Southeast comprised of many islands including Indonesia, Philippines, and Papua New Guinea; Mori et al. 2004; Biasutti et al. 2012). The Bay of Bengal and its adjacent coastal regions also exhibit a strong diurnal variation, introduced by the propagation of convective systems that initiate near the coastal region and then migrate offshore (Zuidema 2003; Liu et al. 2008).

These systematic changes in diurnal variation are also observed inland. Differential heating between elevated terrain and the plains can develop mesoscale convective systems that migrate and lead to a systematic variation in the diurnal cycle (Kikuchi and Wang 2008; Biasutti et al. 2012). For example, the characteristic diurnal rainfall peak in the late afternoon over the Rocky Mountains is systematically delayed eastward toward the adjacent Great Plains, as well as with amplified magnitude under the influence of the nocturnal low-level jet (Bonner 1968; Stensrud 1996; Carbone et al. 2002; Lee et al. 2007b, c; Carbone and Tuttle 2008; Matsui et al. 2010).

Reproduction of those observed features in the diurnal cycle of rainfall remains as a challenge for current general circulation model (GCM) development (Lin et al. 2000; Yang and Slingo 2001; Betts and Jakob 2002a, b; Neale and Slingo 2003; Collier and Bowman 2004; Dai and Trenberth 2004; Liang et al. 2004; Dai 2006; Lee et al. 2007c; Satoh and Kitao 2013; Yuan et al. 2013). According to previous modeling studies, improvements in the horizontal resolution and the parameterization of model physics (e.g., the deep convection parametrization scheme) appear to be major tasks leading to more reliable simulations of diurnal variation of precipitation (Dai et al. 1999; Liang et al. 2004; Lee et al. 2007a, b; Shin et al. 2007; Wang et al. 2007; Rio et al. 2009; Sato et al. 2009; Koo and Hong 2010; Love et al. 2011; Satoh and Kitao 2013; Jin et al. 2016). For example, high horizontal resolution GCMs have demonstrated an improved

performance in simulating the amplitude and phase of the diurnal cycle of precipitation over complex terrains such as the Maritime Continent, Southeast Asia, Central America, and tropical Africa (Arakawa and Kitoh 2005; Ploshay and Lau 2010). Similarly, simulations of the diurnal precipitation variation over North America improved by increasing the spatial resolution from 2° to 0.5° in the three different atmospheric GCMs, resulting in more accurate convective system propagation patterns over the Rocky Mountains' slope (Lee et al. 2007c).

Nonetheless, the aforementioned studies also evidence fundamental limitations in the models themselves, regardless of horizontal resolution improvements. For instance, the propagation systems did not reach the Great Plains in any of the models tested by Lee et al. (2007c), resulting in failed simulations of nocturnal rainfall over the region. Gelaro et al. (2015) identified similar inaccuracies when applying the non-hydrostatic version of Goddard Earth Observing System version 5 (GEOS-5) atmospheric general circulation model (AGCM) at a 7 km resolution to perform simulations over the Great Plains. Dirmeyer et al. (2012) compared the diurnal variations of precipitation simulated by the Integrated Forecast System (IFS) from the European Center for Medium-Range Weather Forecasts (ECMWF) at high resolution (i.e., up to a 10 km grid spacing) and a 7 km resolution implementation of the Non-Hydrostatic Icosahedral Atmospheric Model (NICAM) from the Japan Agency for Marine-Earth Science and Technology (JAMSTEC). The results show that the resolution difference does not necessarily result in a better diurnal variation in the IFS compared to the NICAM, although the NICAM with explicit representation of deep convection is typically more realistic than the IFS with parameterized convection. The NICAM has been tested at 14, 7, and 3.5 km resolutions and increased resolution has reportedly reduced amplitude and phase errors in most regions except for the open ocean (Sato et al. 2009). This simulation improvement has been attributed to a better representation of the structure and life cycle of inland precipitation systems. However, the highest resolution implementation at 3.5 km tends to exaggerate the inland amplitude (Yashiro et al. 2016).

The results from the aforementioned studies suggest that simply increasing the spatial resolution of the global model is not an absolute solution for the improvement of the diurnal cycle of simulated precipitation. Which has been the case for models tested at horizontal resolutions ranging from 1 to 10 km after having been implemented in resolutions of tens to even hundreds of km resolutions using identical models. The results also show that simulation improvement there is largely model-dependent, which is worthy of a further investigation.

The present study seeks to validate the National Aeronautics and Space Administration's (NASA) GEOS-5

atmospheric GCM simulation of the diurnal precipitation variation in the boreal summer season at a 10 km horizontal resolution. The result from this simulation will then be compared with observations as well as a low-resolution (i.e., 50 km) implementation. The analysis will be focused not only on the validation of the global diurnal cycle of precipitation but at the regional scale. Specifically, this study aimed to determine the degree to which varying resolutions affect the representation of the observed systematic transition of the diurnal variation's amplitude and phase over complex boundary conditions such as those occurring in the Bay of Bengal and the United States Great Plains. The same version of this model has been tested by Gelaro et al. (2015) at a 7 km horizontal resolution, rendering qualitatively similar results from those observed in our implementations for North America.

Section 2 describes the observation data, the model experiments, and the analysis methods employed in this study. Section 3 compares the performance of the model simulation over the global domain in terms of the geographical distribution of the amplitude and phase of the diurnal cycle of precipitation. This section also provides a more in-depth comparison of the simulation at a regional scale for the two case-study regions of the Bay of Bengal and the United States Great Plains. Summary and conclusion are presented in Sect. 4.

2 Data and methodology

This study uses the GEOS-5 global model developed by the NASA Global Modeling and Assimilation Office (GMAO). The model is originally a fully-coupled atmospheric model with interactive ocean and sea ice components, but the observed sea surface temperature (SST) is specified in this study. The atmospheric component model is based on a cubed-sphere dynamical core (Putman and Lin 2007).

The cumulus convection scheme is a modified version of the original Relaxed Arakawa-Schubert (RAS) scheme (Moorthi and Suarez 1992). Major modifications include the choice of the boundary layer top as the convection starting level. The relaxation time scale (i.e., convective adjustment time-scale) is specified as a linear function of height, whereby it changes from 30 min when the convective plume is the shallowest to 12 h when it is deepest. Additionally, any convective plume is required to have a higher entrainment rate than the specified minimum threshold value (Tokioka et al. 1988), if this condition is not met, convection is not triggered off. The minimum threshold is inversely proportional to the maximum allowable plume diameter (Bacmeister and Stephens 2011). The threshold is also state-dependent and randomly determined via a power-law probability distribution function. We encourage interested

readers to refer to Lim et al. (2015) and Seo et al. (2019) for more details on stochastic minimum entrainment rate parameterization.

The large-scale condensation scheme employed in this study is a prognostic version developed by Bacmeister et al. (2006). Moreover, the planetary boundary layer is parameterized by the non-local turbulence scheme of Lock et al. (2000); the radiation scheme is based on Chou and Suarez (1994) for longwave and Chou and Suarez (1999) for shortwave radiation, respectively; the land surface is parameterized based on the catchment scheme by Koster et al. (2000); and the model´s gravity wave drag parameterization is based on Mcfarlane (1987) and Garcia and Boville (1994).

The GEOS-5 model has been integrated for 2 specific years (2005–2006) at two different horizontal resolutions: approximately 50 km (0.6° longitude × 0.5° latitude) and 10 km (0.09° longitude × 0.09° latitude). The model has 72 vertical levels with the top boundary at 0.01 hPa. These two model simulations have the same model configurations except for the horizontal resolution. The maximum allowable plume diameter was set to 450 m in both low- and high-resolution runs. Figure 1 shows the surface elevation above sea level in our analysis domain (20°S–45°N, 0°–360°E) for the diurnal cycle of precipitation in boreal summer (June–August). The simulated total precipitation is the sum of convective and non-convective precipitation from the cumulus convection scheme and the large-scale condensation scheme, respectively. This study also analyzes the wind and moisture fields at 850 hPa to investigate the coupling between precipitation and low-level atmospheric circulation such as the land-sea breeze and the mountain-valley winds.

For the model validation, we used the satellite-derived 3-h frequency precipitation data from the TRMM 3B42 version 6 (Huffman et al. 2007), which have a spatial resolution of 0.25° (latitude) × 0.25° (longitude). TRMM provides a limited spatial coverage between 50°S–50°N and 180°W–180°E. Simulated low-level circulation at 850 hPa was validated with the reanalysis data from the Modern Era-Retrospective Analysis for Research and Applications (MERRA; Rienecker et al. 2011), which have an original resolution of 0.50° (latitude) × 0.67° (longitude). The model verification focused on the simulations for two summer periods in 2005 and 2006.

Since the 24-h cycle was predominant both in the observations and the model simulations, the diurnal cycle of precipitation was defined as the 24-h harmonic in this study, which was derived from the Fourier analysis of the summer-mean 24-h diurnal time series. The amplitude and the peak phase were determined from the 24-h harmonic in each grid point (Lee et al. 2007a, b). A precipitation threshold of 0.1 mm h^{-1} was established, such that areas below this criterion were considered to have no significant diurnal variation and were thus excluded from our study.
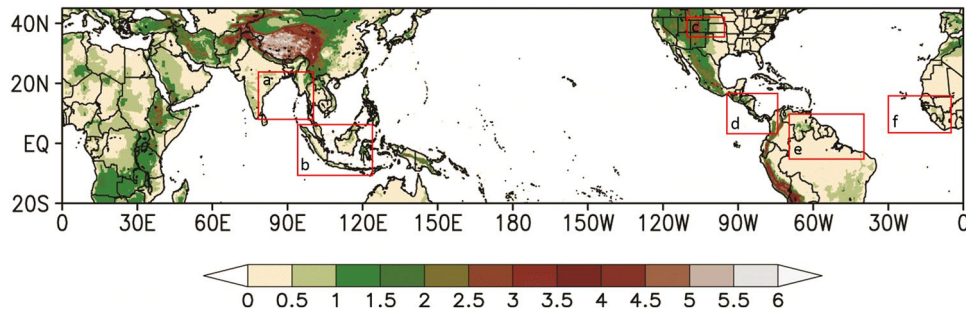
Fig. 1 Surface elevation in the analysis domain. The unit is km. The data are obtained from the United States Navy Fleet Numerical Oceanography Center with an original resolution of 10 min. Red boxes indicate the regions: the Bay of Bengal in South Asia (a, 78°– 100°E, 8°–24°N), the Maritime Continent (b, 95°–125°E, 9°S–6°N), the Great Plains in North America (c, 110°–95°W, 36°–42°N), Central America (d, 95°–75°W, 4°–16°N), South America (70°–40°W, 5°S–10°N), and West Africa (30°–5°W, 3°–15°N)

3 Results and discussion

a. Characteristics of diurnal variation of global precipitation

Observed TRMM summer mean precipitation was compared to the GEOS-5 model simulations at 10 and 50 km horizontal resolutions (hereafter referred to simply as the 10 km and the 50 km models, respectively; Fig. 2). In the observation, most precipitation occurs over the Intertropical Convergence Zones (ITCZs) in the Pacific and the Atlantic, and the Indo-Pacific warm pool region. The observed precipitation is larger over the ocean, except over the land areas influenced by summer monsoons in India, East Asia, and West Africa. Especially, the low-level southwesterly monsoon flow in the Indian subcontinent and South Asia produces a large amount of rainfall in the upstream areas of regions such as the southern foothill of the Himalayas, the west coast of India, the Indochina Peninsula, and the Philippines.
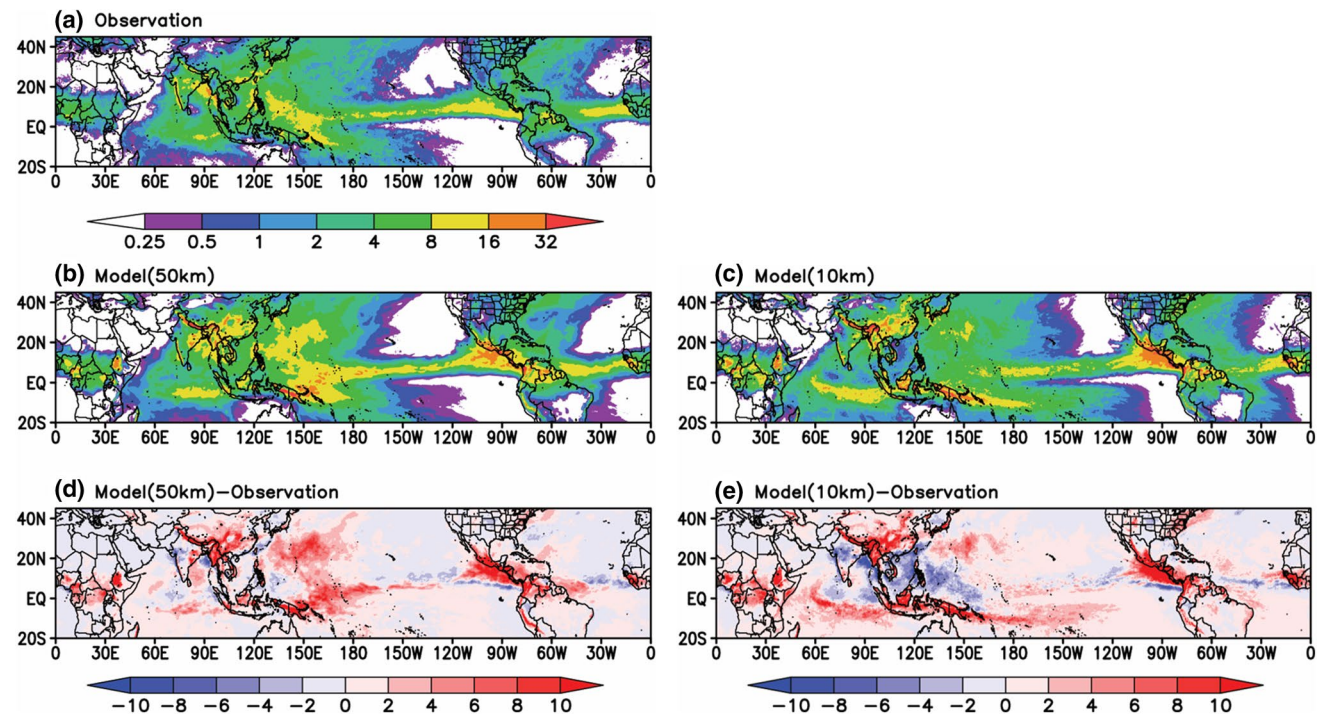
Fig. 2 Time-mean precipitation averaged for two summers (JJA 2005 and 2006) from **a** the TRMM observation and the GEOS-5 model simulation in **b*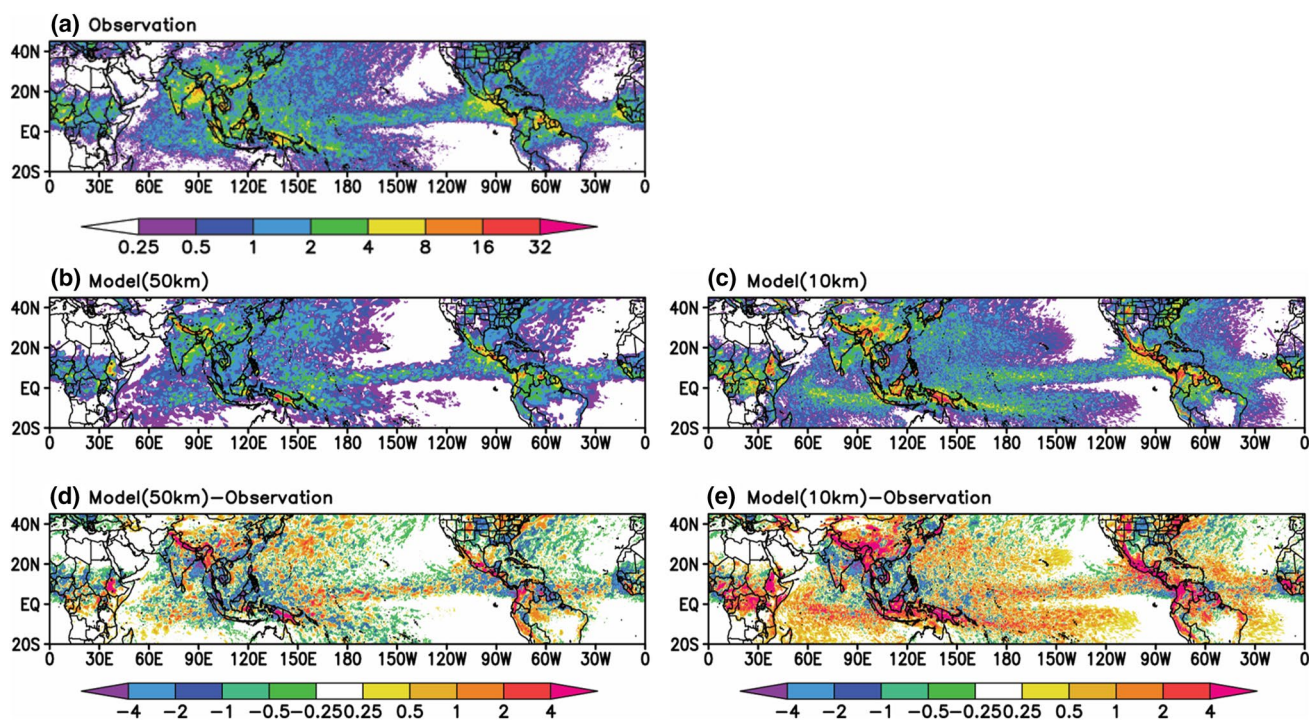* 50 km and **c** 10 km spatial resolution. **d, e** The differences from the observation in the 50-km run and the 10-km run, respectively. The unit is mm day^{-1}

The 50 km model tends to reproduce the basic features of the observed summer mean precipitation pattern realistically (Fig. 2b), albeit with notable discrepancies (Fig. 2d). For instance, the model overestimates the precipitation amount in Africa and China. Also, the ITCZs in the Pacific and the Atlantic are overall weaker in the model simulation, although they are abnormally strong in the eastern ends near the continents. The model generally predicts too much rainfall in the upstream areas of elevated regions such as the Himalayas, the Maritime Continent, the Sierra Madre Occidental (SMO), the Andes, and the elevated inland regions of Africa. These regional and topographical rainfall biases are common in other models, regardless of the difference in the horizontal resolution (Shin et al. 2007; Sato et al. 2009; Dirmeyer et al. 2012; Schiemann et al. 2014).

Overall, the 10 km model (Fig. 2c) shows a similar representation of the summer mean precipitation to the 50 km model, and the bias pattern (Fig. 2e) resembles most of the features appearing in the 50 km model, such as wet biases in Africa and China and more topographical rainfall than the observed in the vicinity of major mountains (Fig. 2d). However, the 10 km model tends to intensify the precipitation biases appearing in the lower resolution implementation, specifically in the Indo-Pacific warm pool region. The resolution increase tends to exaggerate the dry biases in the Bay of Bengal, South China Sea, and the western Pacific,

whereas the wet biases become more severe in the southern Indian Ocean and the Maritime Continent.

Spatial distribution of the amplitude of the diurnal cycle of precipitation was compared between the observation and the model simulations (Fig. 3). The observed pattern (Fig. 3a) is similar to that of the predicted summer mean precipitation (Fig. 2a), particularly on land, indicating that the diurnal cycle is strong where the time-mean precipitation is substantial. Additionally, strong diurnal variation is observed over the adjacent oceans such as the Bay of Bengal, the Maritime Continent, Central America, northeastern Brazil, and the west coast of Africa. These observed features are realistically reproduced by the model simulations at both resolutions. However, both implementations (Fig. 3b, c) show stronger diurnal variation over land, especially near the mountain ranges, where the signal is notably stronger in the 10 km model. This result is consistent with the results from other studies in that the resolution increase in the model tends to overestimate precipitation over mountain ranges (Prein et al. 2016; Pontoppidan et al. 2017). Pontoppidan et al. (2017) showed from their model sensitivity experiments that, as the horizontal resolution of a model increases over complex terrain, the model tends to simulate more localized and stronger vertical motion and moisture perturbations and thereby predicts an increased the topographical rainfall. This suggests that increased

Fig. 3 Amplitude of the diurnal cycle of precipitation obtained from **a** the observation and the model simulation in **b** 50 km and **c** 10 km spatial resolution. **d, e** The differences from the observation in the 50-km run and the 10-km run, respectively. The unit is mm day^{-1}

inhomogeneity introduced by the resolution increase may be largely responsible for topographical rainfall overestimations in most models.

The diurnal cycle over the ocean is also slightly larger in the 10 km model, for instance, in the southern Indian Ocean, the South Pacific Convergence Zone (SPCZ), and the ITCZ. Overall, the differences in diurnal amplitude patterns between the observation and the models (Fig. 3d, e) bear a resemblance to those observed in the time-mean precipitation patterns (Fig. 2d, e). This result suggests that diurnal variation accounts for a considerable portion of the time-mean precipitation. In finding a causal relationship between the diurnal cycle of rainfall and the time-mean precipitation, it is unclear whether the bias of the diurnal cycle contributes to the time-mean bias (Yang and Slingo 2001; Neale and Slingo 2003) or vice versa.

To examine the relationship between the amplitude of the diurnal cycle and the seasonal-mean rainfall amount in more detail, the ratio of the two was compared to the observation and the 50 and 10 km models (Fig. 4). High values indicate that the diurnal cycle is dominant, and it accounts mostly for the seasonal-mean precipitation. The result shows a ratio of over 0.8 in the vicinity of elevated terrains, such as the southern part of the Tibetan Plateau, the eastern part

of the Rocky Mountains, the SMO, the western Andes, the Bay of Bengal, and the Maritime Continent. In general, the 50 km model (Fig. 4b) tends to underestimate the ratio significantly less than the observations in continental regions such as in Africa and the southeastern United States. In contrast, the 10 km model (Fig. 4c) represents it with realistic amplitude in most regions, suggesting that land topography is an important driver for the diurnal cycle of precipitation. Since complex topography can be realistically reproduced as the spatial resolution of the model increases, the resulting high-resolution model exhibits better performance at simulating precipitation caused by large-scale circulation, such as mountain valley winds and sea breeze. Thus, such improvements allow for more realistic simulation of precipitation and its diurnal cycle, which in turn can improve the ratio of the diurnal amplitude to the time-mean precipitation.

When the ratio is averaged over two latitude bands in the subtropics (5°–20°N) and the mid-latitudes (30°–40°N), the observation shows relatively higher values over land and lower values over the ocean. Overall, the 50 km model (Fig. 4d) particularly underestimates the ratio over land, except for the dry regions in mid-latitude Eurasia. The 10 km model (Fig. 4e) improves the simulation significantly with comparable values to the observed, although it
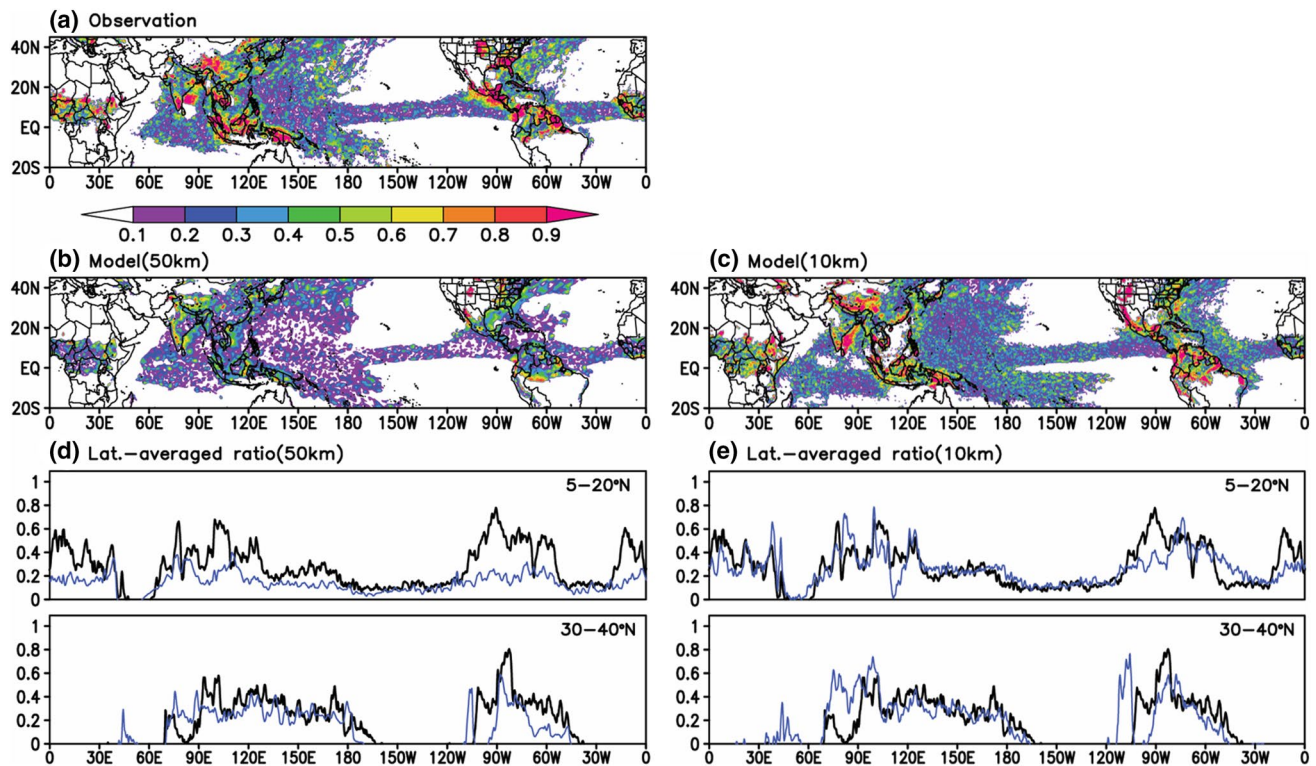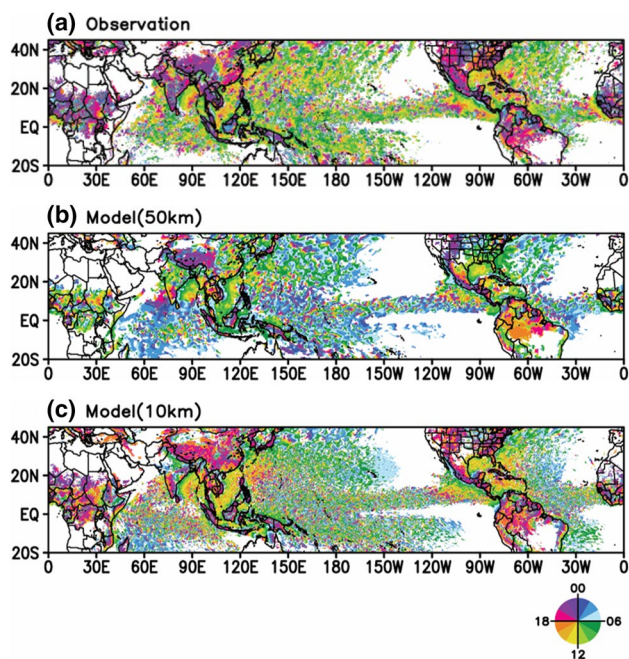

Fig. 4 Ratio of the diurnal cycle amplitude to the time-mean precipitation estimated from **a** the observation and the model simulation in **b** 50 km and **c** 10 km spatial resolution. The areas of time-mean precipitation less than 2 mm day^{-1} are masked out. **d, e** Show the latitude-averaged ratio over the tropics (5°–20°N, upper) and the mid-latitudes (30°–40°N, lower) from the 50 km run and the 10 km run, respectively. Black and blue lines indicate the observation and the model simulation, respectively

tends to describe the ratio unrealistically in some regions, for instance underestimating it over Central America and central Africa in the subtropics and the Great Plains in the mid-latitudes, and overestimating near the Himalayas and the Rockies in the mid-latitudes.

Figure 5 displays the maximum phase (peak hour) of the diurnal cycle of precipitation from the observation and the models. The observation shows the evening or nocturnal peaks of the diurnal precipitation over most of the land areas, in contrast to the morning or afternoon peaks over the ocean and coastal seas. Especially, the peak hours are delayed in the adjacent oceans as one moves away from the coastal line, such as in the Bay of Bengal, the South China Sea. The 50 km model misrepresents the observed maximum phase both over land and the ocean. Diurnal precipitation develops from the morning to the afternoon hours in most of the land regions, exhibiting early phase bias compared with the observations. The diurnal cycle over the open oceans exhibits early phase bias as well, mostly reaching maxima a few hours earlier than observed. The model is able to capture the peak phase transition in the adjacent oceans in the Bay of Bengal, the South China Sea, and the Gulf of Mexico for example, but also with early phase biases. Overall, the 10 km model realistically describes the spatial distribution of the diurnal cycle phase. The contrast in the peak phase between land and ocean is represented more realistically in the 10 km model than in the 50 km model. The diurnal cycle of rainfall
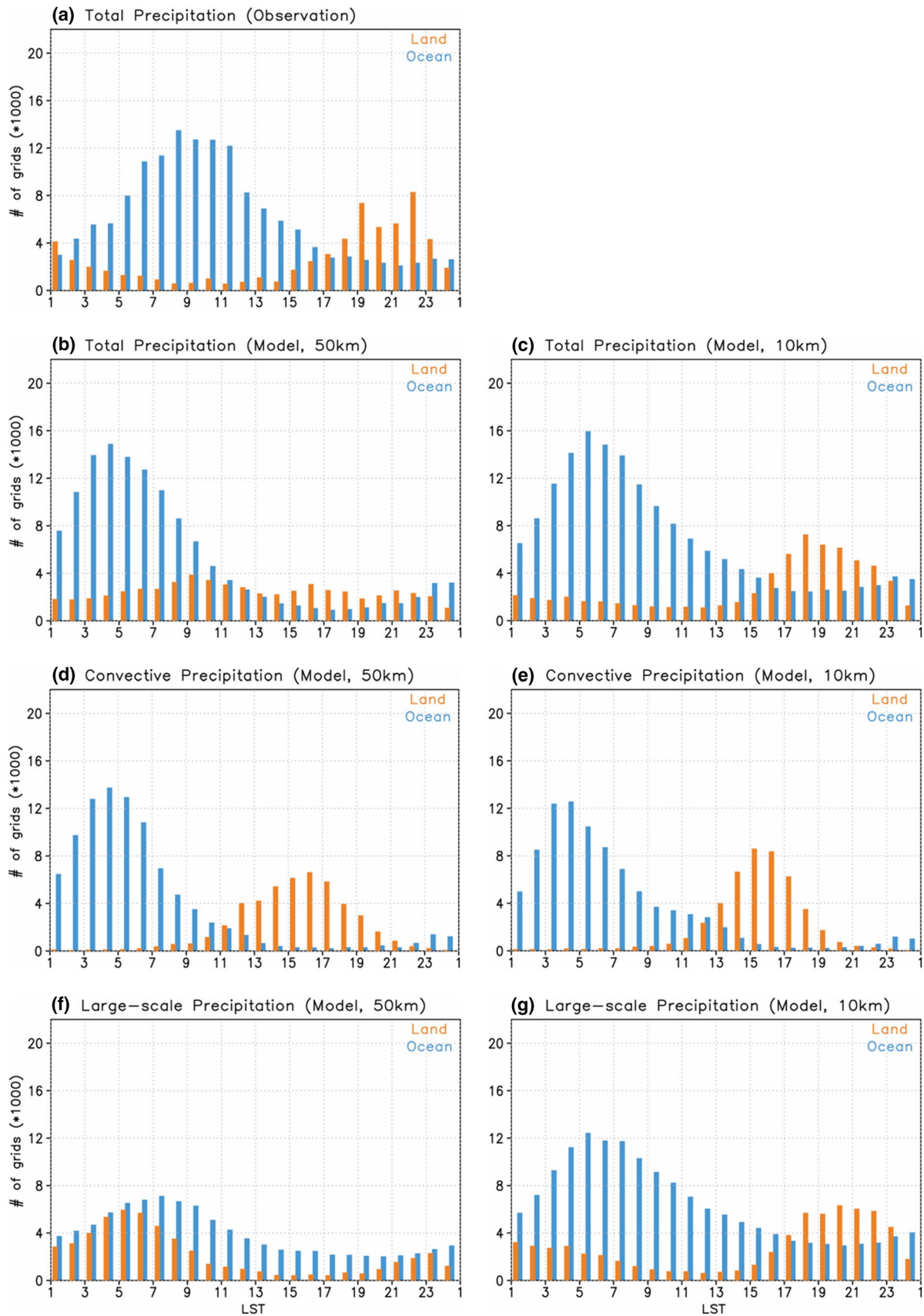

Fig. 5 Peak phase of the diurnal cycle of precipitation as represented in local time obtained from **a** the observation and the model simulation in **b** 50 km and **c** 10 km spatial resolution. The results in grids where the amplitude is under 0.25 mm day^{-1} are excluded

peaks from the evening to midnight in most of the land regions, which aligns well with observations. Additionally, it tends to reproduce the systematic changes in the diurnal cycle phase in the coastal oceans with realistic peak times. This improvement was attributed to a substantial increase in the horizontal resolution of the model, which was sufficient to resolve the propagation of convective systems originated from land. This feature will be revisited in Sect. 3b.

Figure 6 summarizes the diurnal cycle phase in the observations and the 10 km and 50 km models. Here, the peak hour histograms are presented for each instance over the entire land and ocean grid points. The observed precipitation occurs mostly from the evening to the night (i.e., 19–22 LST) over land, and from the morning to the early afternoon (i.e., 06–11 LST) over the ocean, respectively (Fig. 6a). Lee et al. (2007a) explained the differences in the mechanisms responsible for the diurnal variation over land and ocean. On land, surface heating and cooling in the planetary boundary layer is strengthened during daytime and nighttime, respectively, and this leads to a strong diurnal variation. On the other hand, the diurnal variation over the ocean is more affected by nighttime radiative cooling in the upper-level atmosphere. Note that there is a secondary peak at night (i.e., 01 LST) over land in the observation, suggesting the occurrence of regions of nocturnal precipitation peaks such as in the U.S. Great Plains (Dai et al. 2007; Kikuchi and Wang 2008; Sato et al. 2009).

The precipitation over land simulated by the 50 km model exhibits a wide spatial variation in peak time (Fig. 6b), with multiple peaks in the morning (i.e., 09 LST), afternoon (16 LST), and evening (21 LST), failing to reproduce the prevalent evening peaks in the observations. On the other hand, nighttime peaks occurred from 02 to 07 LST in most of the oceans, which is a few hours earlier than observed. The peak hour distribution of the 10 km model closely resembled the observed, including the evening peaks over land (i.e., around 18–19 LST) and the morning peaks over the ocean (i.e., around 05 LST), albeit with simulated peaks occurring a few hours earlier than the observed. The observed precipitation over land tapers off gradually after midnight through the nighttime, a feature represented well in the 10 km model, but not in the 50 km one. Both models did not exhibit much difference in their simulation performance of the diurnal cycle of precipitation over the ocean.

To identify model deficiencies, this study divided total precipitation into convective and large-scale precipitation, according to the parameterized precipitation processes in this model. Both the 50 km and 10 km models show similar responses in convective precipitation over land with maximum peaks around 15–16 LST (c.f. Fig. 6d, e). This convective precipitation is then suppressed in most of the regions during the late evening to early morning (i.e., from 21 to 08 LST) in both models. Conversely, the convective

(a) Total Precipitation (Observation)

(b) Total Precipitation (Model, 50km)

(c) Total Precipitation (Model, 10km)

(d) Convective Precipitation (Model, 50km)

(e) Convective Precipitation (Model, 10km)

(f) Large-scale Precipitation (Model, 50km)

(g) Large-scale Precipitation (Model, 10km)

◄**Fig. 6** Histograms of the peak phase of the diurnal cycle of precipitation over 20°S–40°N. **a** Shows the precipitation from the observation, and **b**, **c** show the simulation results from the 10-km and the 50-km runs, respectively. **d**, **e** Are same as in **b** and **c** except for convective precipitation, and **f**, **g** for large-scale precipitation. Different color bar indicates land (orange), and ocean (blue) points

precipitation over the ocean illustrates the out-of-phase relationship with that over land, with a maximum distribution peak around 03–05 LST. These observations confirm that horizontal resolution change does not affect the behavior of the modeled convective rainfall, as this model does not implement any formulations or parameters that are directly sensitive to the resolution change.

A notable difference between the two simulations was in the large-scale precipitation (Fig. 6f, g). In the 10 km model, the large-scale rainfall develops from late evening to midnight (i.e., 18–24 LST) in most land areas. Considering the histograms for total (Fig. 6c) and convective precipitation (Fig. 6e), large-scale precipitation tends to extend the diurnal precipitation making it last into the evening to help improve the peak phase representation on land. It is also clear that the signal of nocturnal rainfall over land in the 10 km model is entirely attributable to the large-scale precipitation scheme. The responses from convection and large-scale precipitation schemes are somewhat different over the ocean, where the large-scale precipitation develops in phase with the convective precipitation reaching a maximum peak around 04 LST. Therefore, the systematic early phase biases over the ocean in total precipitation are attributed to both the convective and the large-scale precipitation schemes.

The 50 km and 10 km models display substantially different large-scale precipitation simulations. The histogram in Fig. 6f shows the nighttime peaks from 04 to 06 LST over land, while the evening peaks occurring in the 10 km model were less apparent in the 50 km model. This evidently contributes to the phase bias over land in the total precipitation by the 50 km model (Fig. 6b). In our study, the diurnal precipitation by convective and large-scale precipitation over land was somewhat decoupled and independently triggered in the 50 km model, whereas in the 10 km model the two precipitation processes appeared to exhibit feedback, with large-scale precipitation tending to supplement the convective rainfall (see Supplementary Figure S2). Based on these results, it is thought that the phase bias from the low-resolution model is caused by a deficiency in the representation of large-scale precipitation, and the improvement of spatial resolution leads to the more realistic diurnal variation. Over the ocean, the shape of the histograms rendered by the 50 km and 10 km models were similar.

b.   Regional characteristics of the diurnal precipitation

Some regions exhibit a prominent diurnal variation of precipitation. Therefore six regions—the Bay of Bengal, the Maritime Continent, the Great Plains in North America, Central America, South America, and Africa—were selected to examine if GEOS-5 reproduces major features of the observed diurnal variation (Fig. 7). These regions also exhibit a systematic evolution of the diurnal peak due to the propagation of precipitation systems. Before examining these features, we first examined the degree to which the simulations reproduce the domain-averaged diurnal cycle of precipitation by comparing actual diurnal time series. The diurnal variations over land and ocean were separated to elucidate their characteristics in detail.

The observed result indicates that the 24-h diurnal variation is dominant over both land and ocean. The 12-h cycle is not clear in these regions, although it is suggested to be related to the semidiurnal atmospheric tide in the pressure field (Hamilton 1981; Dai 2001) and is typically prominent in open oceans. Generally, precipitation maxima over inland regions occur in the evening (i.e., 18 LST) except in the Great Plains where the positive peak appears at midnight (i.e., 00 LST). The maxima over the ocean are observed generally in the early morning (i.e., 06-09 LST).

The 10 km model reproduces the 24-h diurnal variation with afternoon and morning peaks over land and ocean, respectively, although the slightly early bias is simulated over some inland regions, for instance, the Bay of Bengal and the Great Plains. Shin et al. (2007) indicated similar biases in the five different models investigated in their study. This demonstrates that many models have difficulty in representing the diurnal variation over those regions. The results of the 50 km model show specifically noticeable differences from the 10 km model over land, despite being quite similar over the ocean. The 50 km model ineffectively reproduces the late afternoon rainfall over land in the observation in Southeast Asia, the Maritime Continent, and Africa, although it is more realistic in Central and South America.

Furthermore, the impact of resolution increase is mixed, particularly over land (Fig. 7). The 10 km model tends to exaggerate the diurnal variation of precipitation over land, while the 50 km model shows the opposite. It is well-acknowledged that high-resolution models tend to exaggerate the diurnal cycle compared to lower-resolution versions (e.g., Sato et al. 2009). Yashiro et al. (2016) showed quite consistent results from their global cloud-resolving model tests with no cumulus parameterization. By successively increasing horizontal resolution from 14 to 0.87 km, the nighttime prevalence of rainfall over land in their coarse resolution implementations tended to shift to the afternoon convection more realistically. However, the diurnal cycle amplitude became unrealistically larger. They attributed this to the lack of lateral mixing in deep convective clouds in their cloud-resolving model simulations, but this must not be
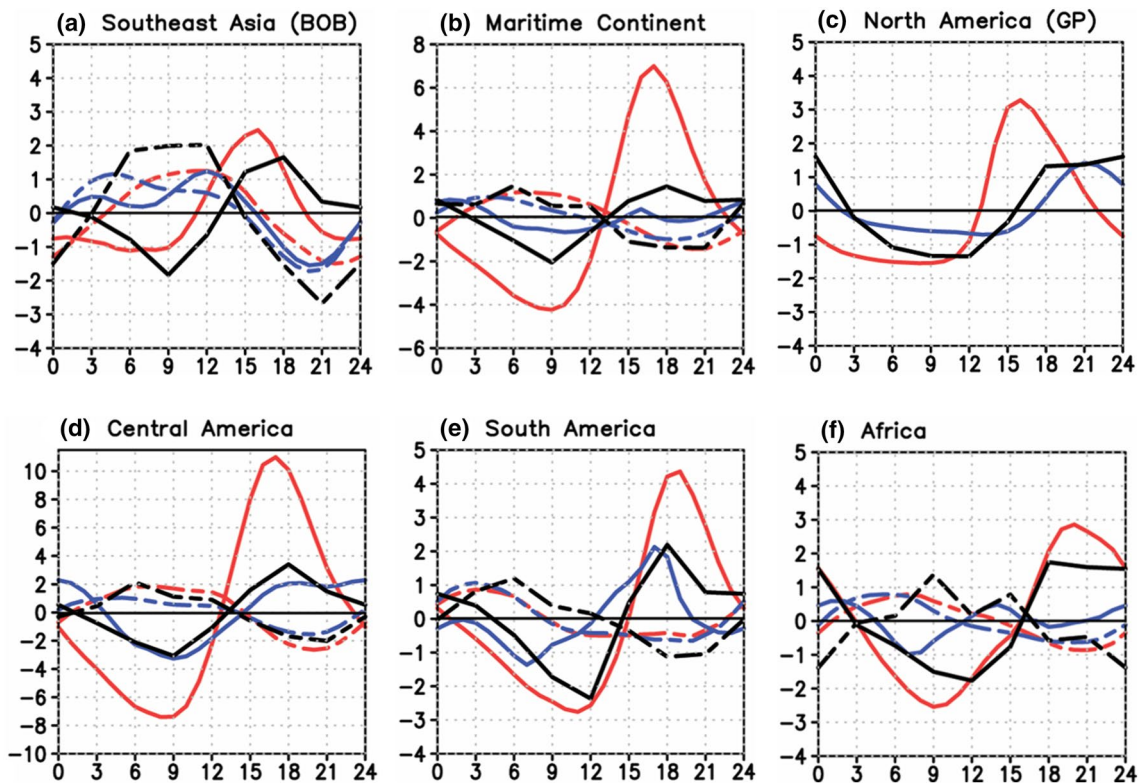
Fig. 7 Diurnal variation of time-averaged precipitation over six regions defined in Fig. 1 from the observation and the model simulations in 50 and 10 km resolution. Black, blue and red lines indicate the observation, the 50-km and the 10-km models, respectively, and solid and dashed lines indicate the average over land and ocean within the boxed regions, respectively. The x-axis shows the local standard time (LST) and the y-axis shows precipitation anomaly (mm day^{-1})

applicable to our GEOS-5 experiments with parameterized deep convection in 50 and 10 km grid spacing.

Although precipitation generally develops more often from late afternoon to evening on land and from night to early morning over the ocean, several regions exhibit more complex features in diurnal variation of precipitation, in which the peak phase of diurnal precipitation maxima tends to change systematically according to the propagation of mesoscale precipitation systems. In this study, two regions were selected for more in-depth analysis to investigate whether the 10 km model can reproduce these features observed in the diurnal cycle.

The Bay of Bengal is a sea surrounded by India and the Indochina Peninsula and features strong diurnal convection that propagates southeastward from the Indian Subcontinent with a 1-day duration (Zuidema 2003; Liu et al. 2008). Figure 8 shows precipitation, 850-hPa wind, and moisture convergence anomalies in the night and afternoon in South Asia, including the Bay of Bengal. In the observation, the precipitation occurs at night over the sea regions of India, the Indochina Peninsula, and the Maritime Continent that are closest to the coast (Fig. 8a). The low-level wind at night flows from the inland region to the ocean, caused by land

surface temperature decreases overnight. In the afternoon (Fig. 8b), precipitation occurs on land because of continental heating by solar radiation during the daytime. Consistently with precipitation anomalies, there are low-level moisture convergence anomalies in the afternoon on land and in the morning over the ocean. The moisture convergence anomalies show a clear contrast between the land and the adjacent oceans. These features are in general consistent with the results presented in Ploshay and Lau (2010), based on a longer 9-year analysis period employing the same TRMM data. The signal of diurnal precipitation also appears in the middle of the Bay of Bengal due to the propagation of the precipitation systems from land (Fig. 9).

The 10 km model accurately reproduces the observed features in this region in terms of the geographical distribution of anomalous precipitation, wind, and moisture convergence during the night (Fig. 8e) and afternoon (Fig. 8f). Positive precipitation anomalies appear over the coastal sea area at night, although with a somewhat weaker magnitude than in the observation. On the other hand, diurnal precipitation anomalies on land are much stronger in the afternoon, such as in Borneo and the Philippines. Additionally, the model tends to portray the
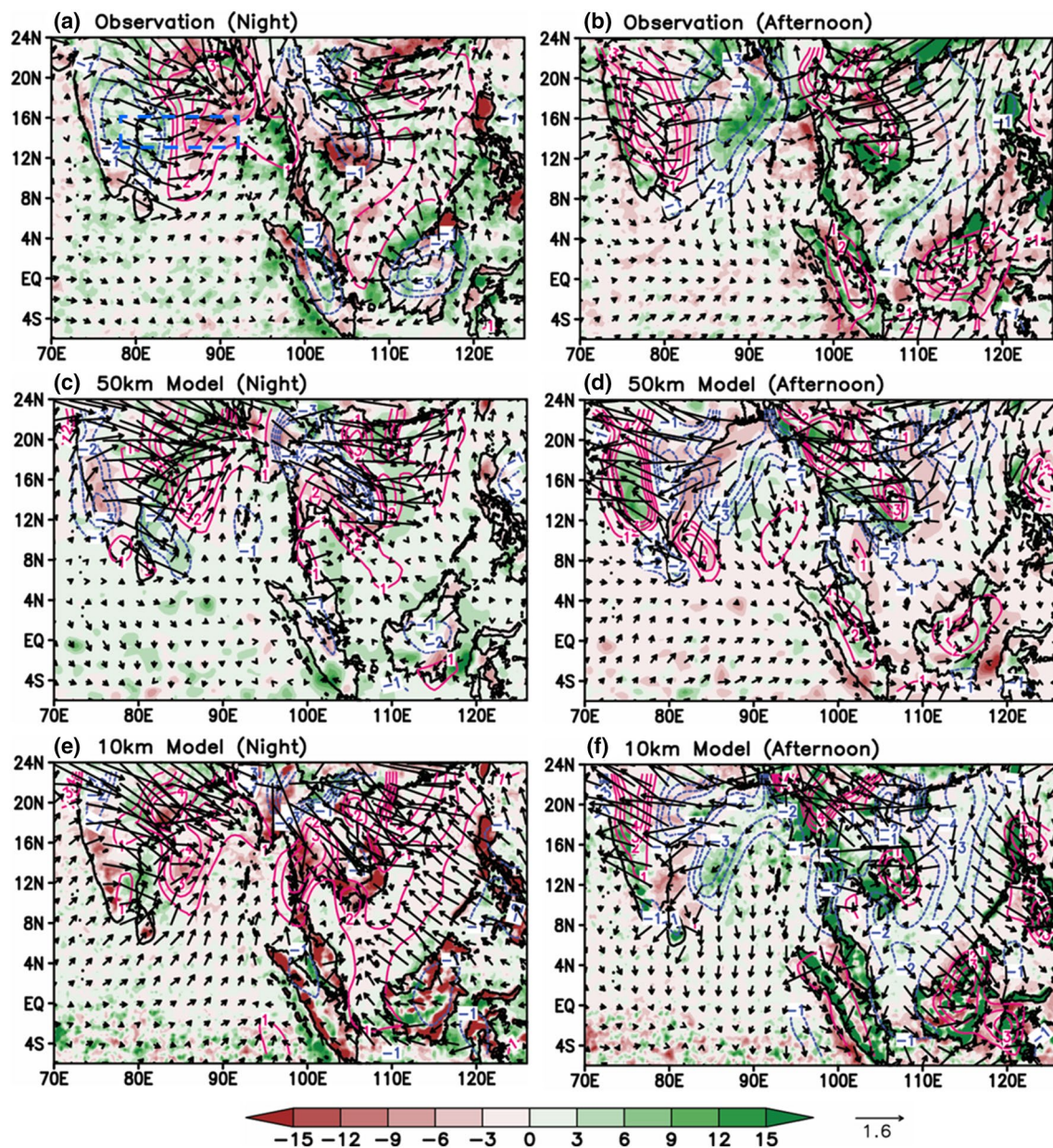
Fig. 8 Spatial distribution of precipitation (shaded, mm day^{-1}) and 850-hPa wind (arrow, m s^{-1}) and moisture convergence (contour, 10^{-5} g kg^{-1} m s^{-1}) anomalies over South Asia from (top) the observation and (middle) the 50-km and (bottom) the 10-km model simulations. **a**, **c**, **e** Show the patterns of wind and moisture convergence in the night averaged for 03 and 06 LST, and **b**, **d**, **f** show the patterns in the afternoon averaged for 15 and 18 LST. Precipitation anomalies are accumulated during 00–06 LST (night), and 12–18 LST (afternoon), respectively. Red (blue) contours indicate the moisture convergence (divergence) anomalies. The blue box in **a** is the analysis region in Figs. 9 and 10

oceanic precipitation anomalies in the middle of the Bay of Bengal as weaker and less organized than in reality. Nevertheless, the diurnal wind pattern was realistically reproduced, and the simulated precipitation anomalies corresponded well with the moisture convergence by the low-level wind. Although the 50 km model (Fig. 8c, d) depicts a similar pattern in a large scale, the simulated moisture convergence over land at daytime was relatively

weaker, for example in the Maritime Continent, where precipitation anomalies exhibited relatively smaller diurnal variation. The nighttime moisture convergence in the adjacent oceans is less clear (e.g., such as in the South China Sea) compared with the reanalysis and the 10 km model. This suggests the 50 km resolution may not be sufficient to represent these local circulation anomalies in the diurnal timescale. In this regard, the GEOS-5 at a 10 km
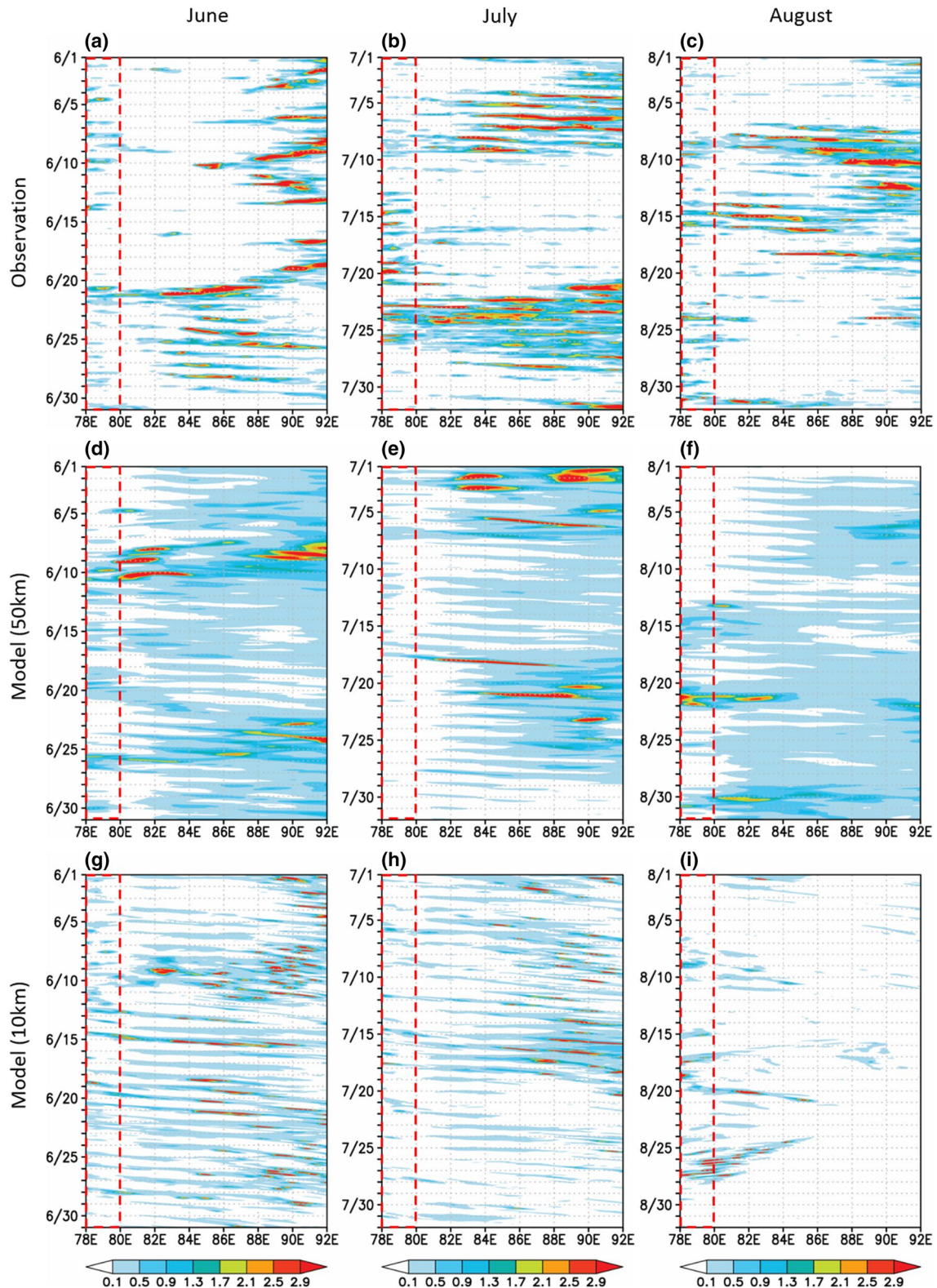
Fig. 9 Time-longitude plots of observed precipitation in the Bay of Bengal in **a** June, **b** July, and **c** August 2005. **d**–**f** Are the 50-km model simulations each month, and **g**–**i** are the 10-km simulations, respectively. The precipitation is averaged over latitude between 13°–16°N, and the unit is mm h^{-1}. Red boxes in dashed line indicate land region over India (78°–80°E)

horizontal resolution better resolves the diurnal wind and associated moisture convergence anomalies in local and regional scales caused by topography and land-sea contrast and improves the diurnal cycle of precipitation.

This study further examines the propagating precipitation systems simulated by the model in the Bay of Bengal. Figure 9 shows the time-longitude plots of precipitation during June–August 2005. The observation shows that the diurnal variation occurs more regularly in the inland region of India. The diurnal precipitation over land occasionally propagates to the adjacent oceans and further eastward to the middle of the Bay of Bengal. This diurnal eastward or southward moving systems are recognized as inertio-gravity waves (Nakazawa 1988; Yang and Slingo 2001; Zuidema 2003). On the ocean side, precipitation variability also occurs in synoptic scales lasting more than a few days, typically in late June–early July. These precipitation systems have been characterized as the convectively-coupled equatorial Kelvin waves (Matsuno 1966; Wheeler and Kiladis 1999). Concurrently, other precipitation systems migrate westward even slowly (e.g., in early June), with propagation speeds corresponding to that of the observed equatorial Rossby waves. These Rossby waves provide an "envelope" of precipitation variability for small-scale individual storms moving eastward (Nakazawa 1988). For a period of 3 months, the observed precipitation over the Bay of Bengal features a pronounced sub-seasonal variability related to the boreal summer intraseasonal oscillation (BSISO, Lawrence and Webster 2002). The intensity of the observed precipitation is stronger over the ocean compared with the coast.

The 50 km model (Fig. 9d–f) reproduces the observed diurnal variation over the whole domain, but the diurnal variation is less pronounced both on land and the adjacent ocean compared with the observations and the 10 km model (Fig. 9g–i). In particular, oceanic precipitation is less connected with the land-initiated convective systems. This suggests that the 50 km resolution is not sufficient to reproduce the eastward propagating convective systems in the form of inertio-gravity waves, although this model represents the synoptic and sub-seasonal convective variability over the ocean. On the other hand, the 10 km model (Fig. 9g–i) tends to delineate the observed summer precipitation and its diurnal variation clearly in the Bay of Bengal, but the model remains broadly distinct from the observation. GEOS-5 simulates precipitation on a more regular basis on land. Also, it tends to propagate eastward to the middle of the Bay of Bengal too often. It was also noted that the sub-seasonal variability in the simulated precipitation is rather weak compared with the observations, although the model tends to simulate the precipitation signals from equatorial Kelvin and Rossby waves. Except for these discrepancies, the model can reproduce the eastward-propagating precipitation systems originated from land.

The observed diurnal precipitation anomalies peaking in the afternoon in the middle of the Bay of Bengal appear to be driven by the propagation systems originated from the inland diurnal convection. Figure 10 shows the regression pattern of precipitation, 850-hPa wind, and its convergence, as a function of LST concerning the precipitation events in the middle of the Bay of Bengal at 15 LST. In the observation (Fig. 10a), the positive precipitation anomalies initiate over land in the evening and move over the center of the Bay of Bengal, reaching peak intensity in the afternoon. Moreover, the convergence of low-level wind anomalies leads the precipitation signal, whereas the wind divergence appears in the precipitation region. This suggests that the diurnal cycle of precipitation in the Bay of Bengal is manifested by the eastward propagation of convectively-coupled inertio-gravity waves (Zuidema 2003; Matsui et al. 2010).

Both the 50 km (Fig. 10b) and 10 km models (Fig. 10c) tend to reproduce this observed propagation pattern realistically, although the eastward propagation shows a more realistic association with the diurnal variation on land in the 10 km model. Another model deficiency is in the low-level wind convergence, where the model simulates precipitation anomalies in phase with the low-level convergence, unlike in the observations, suggesting that the simulated diurnal precipitation anomalies are coupled tightly with low-level wind convergence. Previous studies pointed out that the phase difference between low-level wind convergence and convection is critical for the development and propagation of waves (Wang 2005; Wang and Chen 2017). Unrealistic, in-phase relationships between wind convergence and precipitation in the model simulations might be responsible for the weak amplitude and damping in the propagating precipitation systems. Indeed, the simulated precipitation anomalies decay faster than the observed ones and rarely reach the eastern part of the Bay of Bengal (93°E).

Another region exhibiting a pronounced diurnal precipitation signal is the east of the Rocky Mountains and the Great Plains in North America. The maximum precipitation anomaly peaks occurred in the late afternoon or the early evening over most of the inland regions, and at midnight over the Great Plains, as shown in Fig. 7. Figure 11 displays the observed and the simulated precipitation, 850-hPa wind and moisture convergence anomalies in the contiguous United States and northern Mexico in the afternoon and night. In the afternoon, diurnal precipitation increases in the southeastern United States and the east side of the Rockies (Fig. 11a). Diurnal winds blow from the eastern region of North America to the elevated terrain of the eastern Rockies, which causes differential heating in these mountainous regions. Low-level moisture convergence is in phase with the positive precipitation near the mountains (e.g., the Rockies, the SMO, and the southeastern United States). In contrast to the afternoon, precipitation anomalies develop over the
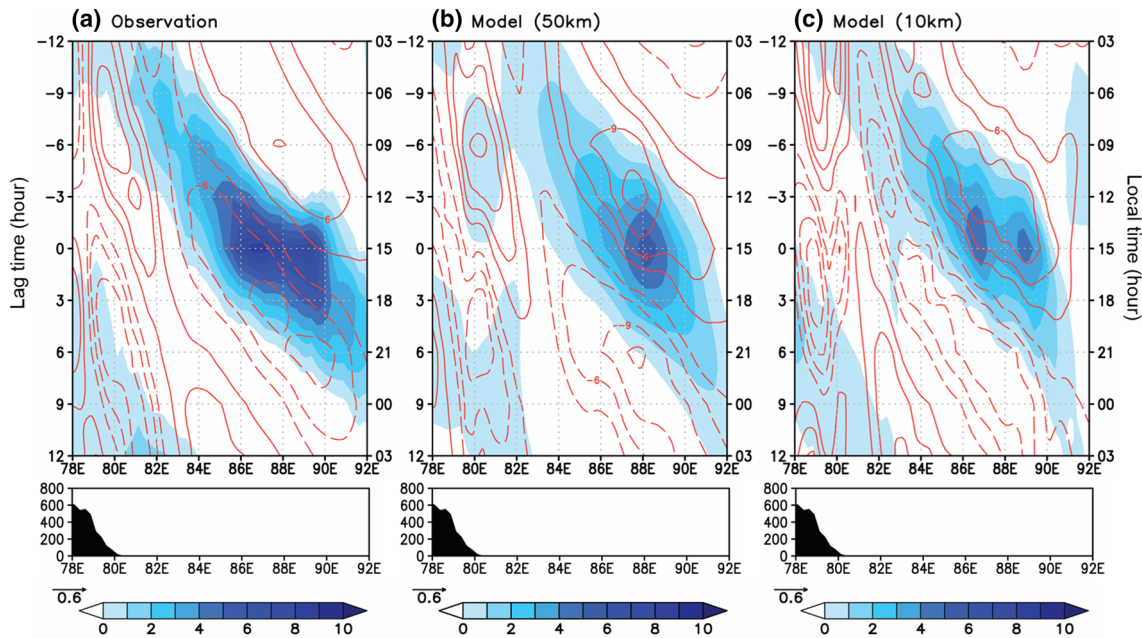
Fig. 10 Lag time—longitude plots of precipitation (shaded) and convergence at 850 hPa (contour) anomalies in **a** the observation, **b** the 50-km, and **c** the 10-km model simulations. The values are obtained from the regression with a reference time series of precipitation anomaly averaged over the central part of the Bay of Bengal (86°–90°E, 13°–16°N), and averaged over 13°–16°N. Surface elevation is presented in the bottom panels. The units of precipitation and convergence are mm h^{-1} and 10^{-7} s^{-1}, respectively

Great Plains at night, accompanied by low-level southerlies associated with the active phase of the Great Plains Low-Level Jet (GPLLJ; Higgins et al. 1997; Fig. 11b). The low-level moisture convergence driven by the GPLLJ appears over the region with positive precipitation anomalies. Previous studies suggest that the GPLLJ transports moisture from the Gulf, thereby providing a more favorable condition for moisture convergence and precipitation events in the Great Plains (Jiang et al. 2007; Pu and Dickinson 2014). At this point, diurnal precipitation is suppressed in the southeastern United States.

Overall patterns in the diurnal precipitation and winds are reproduced properly by the 10 km model (Fig. 11e, f), which is demonstrated by its realistic depiction of precipitation anomalies in the southeastern United States. However, the model tends to overestimate precipitation in the vicinity of an elevated terrain such as in the Rockies and the SMO in the afternoon. Both models reproduce the observed downward propagation of precipitation anomalies, initiated in the mountains in the afternoon and moving to the Gulf of California at night (Lee et al. 2007c) with much stronger amplitude; this pattern is particularly noticeable in the 10 km model. Simulated wind anomalies are unrealistically strong toward these regions in both models. The most prominent deficiency in the model is the very weak precipitation signal at nighttime over the Great Plains (Fig. 11d, f), even though the nocturnal GPLLJ from the Gulf of Mexico is reasonable. Indeed, the 10 km model shows a realistic diurnal variation

of moisture convergence anomalies such as convergence along the Rockies and divergence in the Southern Plains in the afternoon and their reversals at night. On the other hand, the 50 km model inaccurately reproduced moisture convergence anomalies in the Great Plains at nighttime, where the main region of convergence was simulated weaker and unrealistically further northeastward compared with the observations (Fig. 11d). A similar discrepancy can be found in Dirmeyer et al. (2012). They indicated that the models in both very high and low spatial resolution do not adequately simulate the nocturnal precipitation anomalies over the Great Plains. Although they attributed this to an unrealistically weak vertically-integrated moisture transport to the region, this is likely not the case in our experiments, particularly in the 10 km model which shows realistic moisture convergence anomalies during the night. This may suggest a fundamental limitation in the representation of observed mesoscale convective systems even at a 10 km resolution.

Figure 12 shows the time-longitude precipitation plots from the observed and simulated data across the eastern Rockies and the adjacent Great Plains. There is a robust signal of eastward propagation from the elevated terrain to the flat regions in the east toward the Great Plains in the observation. This signal is quite regular, except in mid- to late-July 2005 (Fig. 12a–c). The 50 km model (Fig. 12d–f) was notoriously inaccurate at representing both the diurnal variation over the Rockies and its occasional eastward propagation toward the Great Plains. At this resolution, the
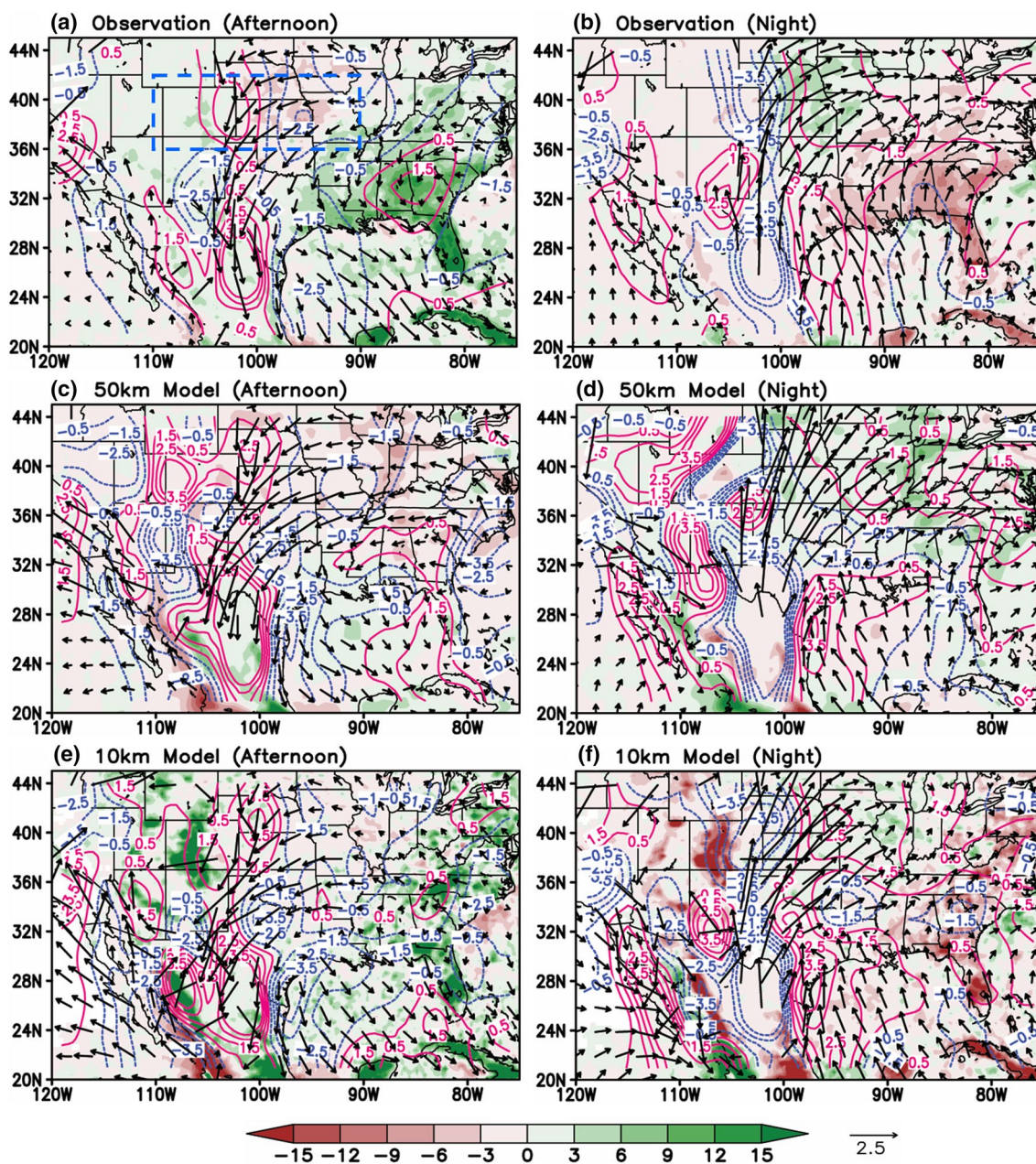
Fig. 11 Same as Fig. 8 except for North America. **a, c, e** Show the patterns of wind and moisture convergence in the afternoon averaged for 12 and 15 LST, and **b, d, f** show the patterns in the night averaged for 00 and 03 LST. Precipitation anomalies are accumulated during 12–18 LST (afternoon) and 00–06 LST (night), respectively. The blue box in **a** is the analysis region in Figs. 12 and 13

diurnal variability in the mountains and the plains appear separated in most cases. The 10 km simulation (Fig. 10g–i) agrees well with the observations that diurnal precipitation is initiated in the Rockies and propagates eastward toward the Great Plains. However, the simulated diurnal variation over the Rockies is both too frequent and strong compared with the observations. Although the propagating feature of the model is somewhat realistic in June and July, this signal is quite suppressed in the model during most of August (Fig. 12i). This leads to a weak diurnal cycle of precipitation

in the Great Plains, and it seems to be responsible for the dry bias of this model in the Great Plains (105°–95°W). Further, it was found that the frequency of the simulated precipitation over the Great Plains (about 0.14 day^{-1}) is roughly half of the observed frequency (about 0.31 day^{-1}). It is also worth noting that the propagation speed was slower in the 10 km model than the observed. Previous studies have speculated that it seems to be related to model deficiencies in the consideration of the vertical distribution of moist static energy and the diabatic heating simulated by the parameterized
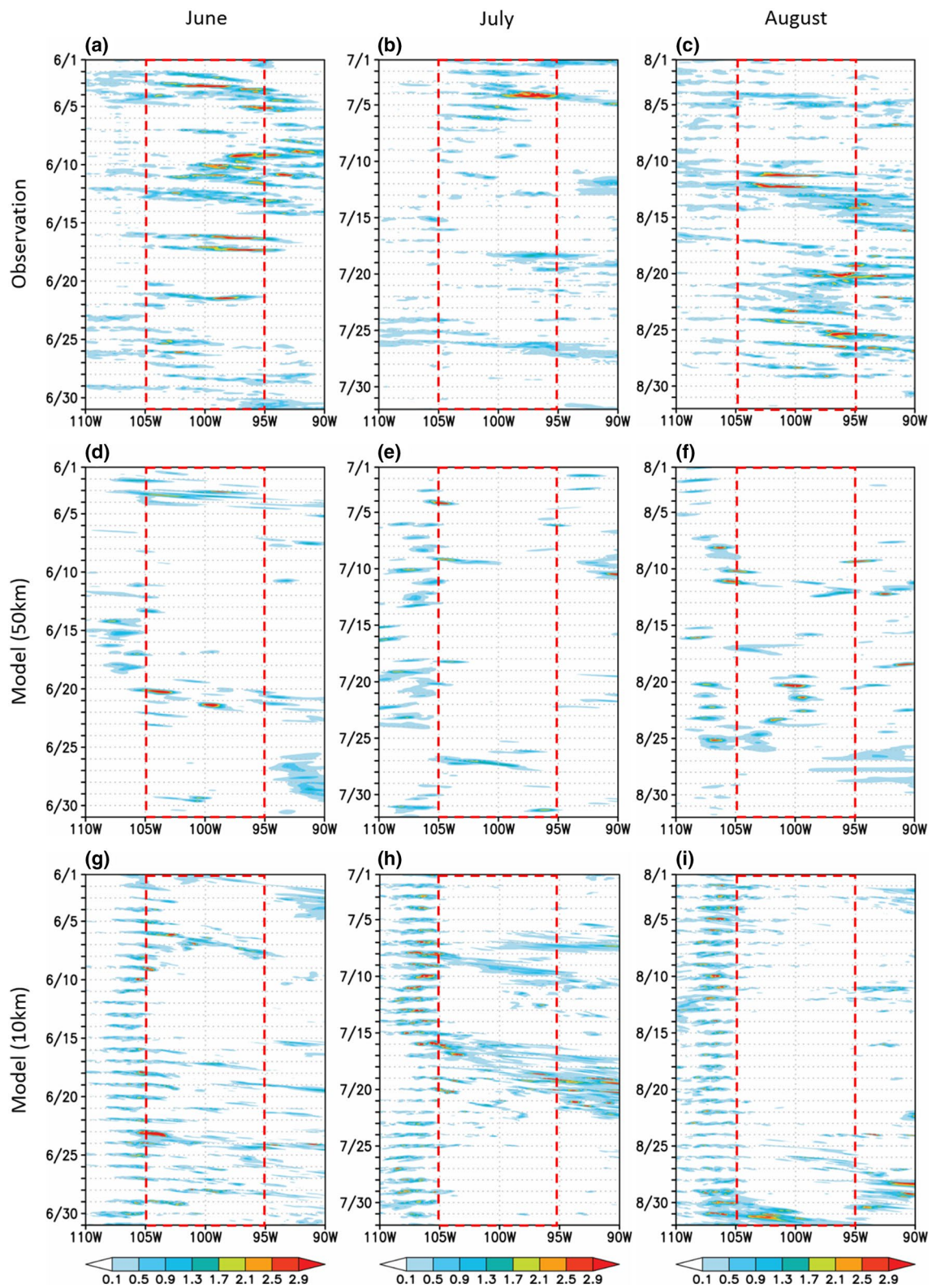
Fig. 12 Same as Fig. 9 except for the results averaged over the Great Plains (36°–42°N). Red boxes in dashed line indicate Great Plains region (105°–95°W)

deep convection scheme. From the long-term analysis of assimilated rainfall data based on radar and rain gauge networks over the United States, Matsui et al. (2010) suggested that the observed rainfall propagation speed can be simply scaled by the square root of the convective available potential energy (CAPE). This is consistent with the moist gravity wave theory and the analytical model results by Moncrieff and Miller (1976). A more comprehensive comparison between observed data and model simulations integrating CAPE and diabatic heating are needed and may become the focus of a future study.

Figure 13 shows the regression patterns of precipitation, 850-hPa wind, and its convergence over the Rockies and the adjacent Great Plains, as a function of LST regarding the nocturnal precipitation in the Great Plains. In the observation (Fig. 13a), the diurnal precipitation is initially developed in the top of the mountains in the afternoon, and then the precipitation signal propagates east and west down the slope. In particular, the eastward propagating signal tends to be stronger with full strength at 100°–95°W at roughly midnight (i.e., 00 LST). Over the Great Plains, the observed moisture convergence anomalies show the in-phase relationship with the diurnal precipitation (Fig. 13a). This is consistent with previous studies that have attributed the nocturnal low-level moisture convergence to the strong southerlies developing in the nighttime associated with the GPLLJ.

Although the 10 km model (Fig. 13c) performs better than the 50 km model (Fig. 13b) in terms of initiation over the mountains and downslope propagation toward the Great

Plains, it is still notably biased. Diurnal precipitation falls mostly over the Rockies. Although the model tends to simulate nighttime precipitation over the Great Plains, this signal is much weaker compared with the observations. This is largely due to the rare connection with the eastward propagating signal from the Rockies as shown in Fig. 12. The low-level moisture convergence is either weak in the 50 km model, or less organized in the 10 km model.

4 Summary and conclusion

This study examines the realism of the diurnal variation of warm-season precipitation simulated by the GEOS-5 AGCM at a 10 km horizontal resolution. Our study sought to determine the level of improvements that could be expected in this model in terms of its capacity to accurately simulate the amplitude and phase of the diurnal cycle of precipitation. In particular, our research focused on whether the model could adequately reproduce the observed precipitation systems in local and regional scales that propagated and produced systematic changes in the amplitude and phase of the diurnal cycle in complex terrains such as in the Bay of Bengal in South Asia, and the vicinity of the Rockies and adjacent Great Plains. By comparing the 50 and 10 km models, we could elucidate the potential improvements and fundamental limitations of the 10 km model in detail.

The 10 km model simulates a realistic summer mean precipitation pattern over the global domain. Several
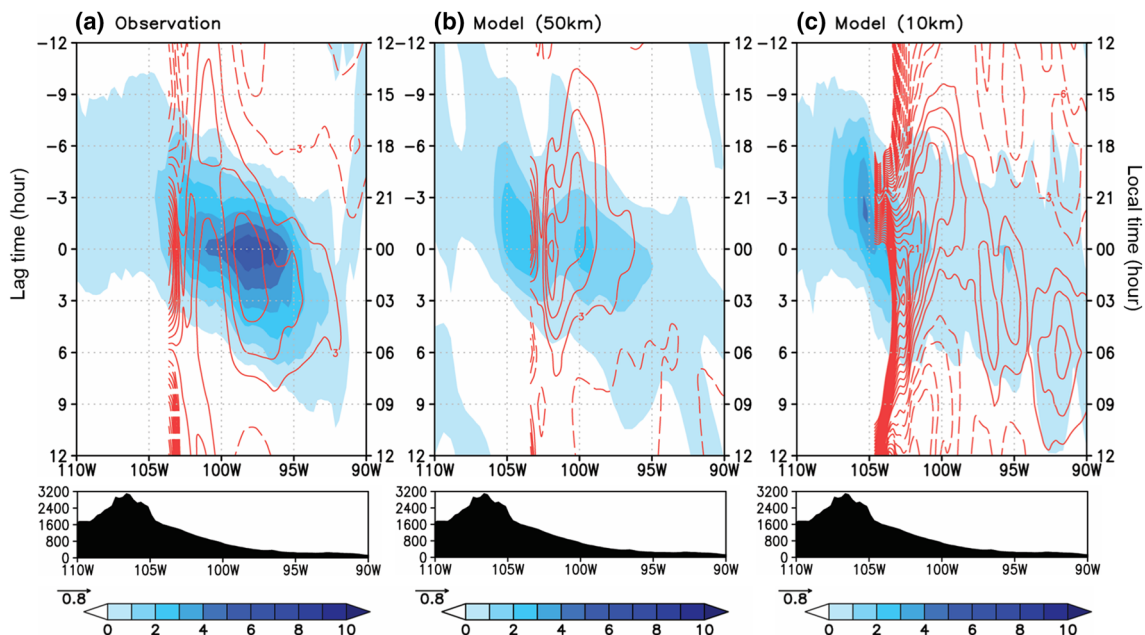
Fig. 13 Same as Fig. 10 except for North America. The reference time series of precipitation anomaly is obtained over the Great Plains (105°–95°W, 36°–42°N), the values are the average of 36°–42°N

deficiencies were also highlighted though, such as the precipitation overestimation over the elevated regions in the Himalayas, the Rockies, the SMO, and the Andes, and underestimation in the Indian Ocean and the SPCZ. Overall, the diurnal cycle of precipitation in the 10 km model was realistic in terms of the spatial distribution of the amplitude and peak phase. In particular, the phase of the diurnal cycle of precipitation was remarkably well simulated, and the 10 km model reproduces the correct timing of diurnal precipitation on land in many locations. The simulated total precipitation on land exhibits realistic evening peaks in general, where the parameterization of large-scale precipitation process represents the diurnal phase of precipitation correctly, rather than the parameterization of deep convection that drives the maximum precipitation in the early afternoon. On the other hand, it simulates the peak time for oceanic precipitation roughly 5 h earlier than the observations. The simulation is also realistic in the six selected regions in the globe where the observation shows pronounced diurnal variation. The 24-h cycle is predominant in those regions, particularly over land, both in the observation and in the 10 km model.

The 10 km model is also capable of reproducing the systematic changes in the observed diurnal cycle phase in the vicinity of complex terrains. This study further investigated the diurnal variation in the Bay of Bengal and the Great Plains in the United States in the context of precipitation system propagation. In Southeast Asia, the diurnal precipitation variation induced by the land-sea thermal contrast is realistically reproduced by the model as well as the associated low-level diurnal wind anomalies in local and regional scales. Especially, the precipitation systems originally initiated in the Indian Subcontinent and propagating to the middle of the Bay of Bengal are depicted realistically by the model. Nevertheless, the model shows a notable deficiency in the eastern Rockies and the adjacent Great Plains. The model had a limited capability to simulate nocturnal precipitation in the Great Plains, even though the low-level circulation and moisture convergence anomalies associated with the GPLLJ are represented realistically. The diurnal cycle of precipitation was simulated too strongly over the mountains, and the eastward propagation of precipitating systems was unrealistically confined to the west of the Continental Divide.

In summary, the increase of the horizontal resolution of the global climate model to a 10 km resolution significantly improved the representation of the diurnal cycle of precipitation in our GEOS-5 model experiments. It is noted, however, that this improvement can be model-dependent. Although the increase of horizontal resolution can substantially improve the representation of local- and regional-scale circulations such as land-sea breeze and mountain-valley topographic circulation, as would be expected from any model, the simulation differences across the models implemented at comparable 10 km resolution or higher suggest that the parametrizations of moist physics is likely the major source of uncertainty and the model diversity (Sato et al. 2009; Dirmeyer et al. 2012; Yashiro et al. 2016). The improvements in the GEOS-5 model seem to be largely related to the enhanced contribution of the large-scale precipitation parameterization. As the observed precipitation has a variety of initiation mechanisms, the conventional parameterization of deep convection based on a column instability may be limited in reflecting those mechanisms. The GEOS-5 model employs the convective parameterization scheme, constraining deep convection based on the stochastic limit of minimum cumulus entrainment (Lim et al., 2015). This makes the convective and the large-scale precipitation comparable in magnitude both in the 50 km and the 10 km models (see Supplementary Figure S1), which is also consistent with the estimate from the TRMM observation (Schumacher and Houze 2003). While convective precipitation is driven by boundary layer heating and the increase of CAPE (Moorthi and Suarez 1992), the large-scale precipitation is determined by the increase of relative humidity in this model (Bacmeister et al. 2006), as in most of the global models. Moisture convergence is one of the dominant processes that drive condensation and precipitation in the model, and this seems to help enhance the coupling between circulation and precipitation, as observed in the propagation process of precipitation anomalies over the Bay of Bengal. Furthermore, this mechanism seems to depend on model resolution. The suppression of deep convection by the stochastic limit of minimum cumulus entrainment in the 50 km model merely suppresses daytime precipitation over land, and the simulation features less prominent propagation of precipitation systems, presumably due to horizontal resolution limitation.

Despite the remarkable improvements in representing the geographical features of the diurnal cycle of warm-season precipitation, the high-resolution model still exhibits intrinsic limitations. The bias of excessive precipitation over the elevated terrains becomes even worse in the higher resolution implementation, which seems to be common in other global and regional models. These regions feature exceptionally strong diurnal variation of precipitation, suggesting that the time-mean precipitation bias is largely associated with the bias in the diurnal cycle of local circulations and precipitation. A more diagnostic approach is needed to understand the underlying physical and dynamical processes and how the increase of inhomogeneity in the boundary condition could drive large accumulated rainfall over small confined areas.

This study also highlights the fact that the model deficiencies in the continental inland regions such as the United States Great Plains are not removed completely by the increase of the horizontal resolution up to 10 km resolution or similar. Thus, more in-depth analysis and more rigorous

modeling methods are required to understand the interactions between mesoscale convective systems, complex terrains, and large-scale circulations.

References

Arakawa O, Kitoh A (2005) Rainfall diurnal variation over the indonesian Maritime Continent simulated by 20 km-mesh GCM. Sola 1:109–112

Bacmeister JT, Stephens G (2011) Spatial statistics of likely convective clouds in CloudSat data. J Geophys Res Atmos. https://doi.org/10.1029/2010JD014444

Bacmeister JT, Suarez MJ, Robertson FR (2006) Rain reevaporation, boundary layer–convection interactions, and Pacific rainfall patterns in an AGCM. J Atmos Sci 63:3383–3403

Betts AK, Jakob C (2002a) Study of diurnal cycle of convective precipitation over Amazonia using a single column model. J Geophys Res 107(D23):4732

Betts AK, Jakob C (2002b) Evaluation of the diurnal cycle of precipitation, surface thermodynamics, and surface fluxes in the ECMWF model using LBA data. J Geophys Res 107(D20):8045

Biasutti M, Yuter SE, Burleyson CD, Sobel AH (2012) Very high resolution rainfall patterns measured by TRMM precipitation radar: seasonal and diurnal cycles. Clim Dyn 39:239–258

Bonner WD (1968) Climatology of low level jet. Mon Weather Rev 96:833–850

Carbone RE, Tuttle JD (2008) Rainfall occurrence in the US warm season: the diurnal cycle. J Clim 21:4132–4146

Carbone RE, Tuttle JD, Ahijevych DA, Trier SB (2002) Inferences of predictability associated with warm season precipitation episodes. J Atmos Sci 59:2033–2056

Chou MD, Suarez MJ (1994) An efficient thermal infrared radiation parameterization for use in general circulation models. NASA Technical Memorandum 104606, vol 3. NASA, Goddard Space Flight Center, Greenbelt, Maryland

Chou MD, Suarez MJ (1999) A solar radiation parameterization for atmospheric studies. NASA Technical Memorandum 104606, vol 15. NASA, Goddard Space Flight Center, Greenbelt, Maryland

Collier JC, Bowman KP (2004) Diurnal cycle of tropical precipitation in a general circulation model. J Geophys Res 109:D17105

Dai A (2001) Global precipitation and thunderstorm frequencies. Part II: diurnal variations. J Clim 14:1112–1128

Dai A (2006) Precipitation characteristics in eighteen coupled climate models. J Clim 19:4605–4630

Dai A, Trenberth KE (2004) The diurnal cycle and its depiction in the Community Climate System Model. J Clim 17:930–951

Dai A, Giorgi F, Trenberth KE (1999) Observed and model-simulated diurnal cycles of precipitation over the contiguous United States. J Geophys Res 104:6377–6402

Dai A, Lin X, Hsu KL (2007) The frequency, intensity, and diurnal cycle of precipitation in surface and satellite observations over low- and mid-latitudes. Clim Dyn 29:727–744

Dirmeyer PA et al (2012) Simulating the diurnal cycle of rainfall in global climate models: resolution versus parameterization. Clim Dyn 39:399–418

Garcia RR, Boville BA (1994) Downward control of the mean meridional circulation and temperature distribution of the polar winter stratosphere. J Atmos Sci 51:2238–2245

Gelaro R et al (2015) Evaluation of the 7-km GEOS-5 nature run. NASA Technical Memorandum 104606, vol 36. NASA, Goddard Space Flight Center, Greenbelt, Maryland

Hamilton K (1981) A note on the observed diurnal and semidiurnal rainfall variations. J Geophys Res 86(C12):12122–12126

Higgins RW, Yao Y, Yarosh ES, Janowiak JE, Mo KC (1997) Influence of the great plains low-level jet on summertime precipitation and moisture transport over the central United States. J Clim 10:481–507

Huffman GJ, Bolvin DT, Nelkin EJ, Wolff DB, Adler RF, Gu G, Hong Y, Bowman KP, Stocker EF (2007) The TRMM multisatellite precipitation analysis (TMPA): quasi-global, multiyear, combined-sensor precipitation estimates at fine scales. J Hydrometeorol 8:38–55

Jiang XN, Lau NC, Held IM, Ploshay JJ (2007) Mechanisms of the great plains low-level jet as simulated in an AGCM. J Atmos Sci 64:532–547

Jin EK, Choi IJ, Kim SY, Han JY (2016) Impact of model resolution on the simulation of diurnal variations of precipitation over East Asia. J Geophys Res 121:1652–1670

Kikuchi K, Wang B (2008) Diurnal precipitation regimes in the global tropics. J Clim 21:2680–2696

Koo MS, Hong SY (2010) Diurnal variations of simulated precipitation over East Asia in two regional climate models. J Geophys Res 115:D05105

Koster RD, Suarez MJ, Ducharne A, Stieglitz M, Kumar P (2000) A catchment-based approach to modeling land surface processes in a general circulation model: 1. Model structure. J Geophys Res 105(D20):24809–24822

Lawrence DM, Webster PJ (2002) The boreal summer intraseasonal oscillation: relationship between northward and eastward movement of convection. J Atmos Sci 59:1593–1606

Lee MI, Schubert SD, Suarez MJ, Bell TL, Kim KM (2007a) Diurnal cycle of precipitation in the NASA seasonal to interannual prediction project atmospheric general circulation model. J Geophys Res 112:D16111

Lee MI, Schubert SD, Suarez MJ, Held IM, Lau N, Ploshay JJ, Kumar A, Kim H, Schemm JE (2007b) An analysis of the warm-season diurnal cycle over the continental united states and northern Mexico in general circulation models. J Hydrometeorol 8:344–366

Lee MI, Schubert SD, Suarez MJ, Held IM, Kumar A, Bell TL, Schemm JE, Lau N, Ploshay JJ, Kim H, Yoo S (2007c) Sensitivity to horizontal resolution in the AGCM simulations of warm season diurnal cycle of precipitation over the United States and northern Mexico. J Clim 20:1862–1881

Liang XZ, Li L, Dai A, Kunkel KE (2004) Regional climate model simulation of summer precipitation diurnal cycle over the United States. Geophys Res Lett 31:L24208

Lim YK, Schubert SD, Reale O, Lee MI, Molod AM, Suarez MJ (2015) Sensitivity of tropical cyclones to parameterized convection in the NASA GEOS-5 model. J Clim 28:551–573

Lin X, Randall DA, Fowler LD (2000) Diurnal variability of the hydrologic cycle and radiative fluxes: comparisons between observations and a GCM. J Clim 13:4159–4179

Liu CH, Moncrieff MW, Tuttle JD (2008) A note on propagating rainfall episodes over the Bay of Bengal. Q J R Meteorol Soc 134:787–792

Lock AP, Brown AR, Bush MR, Martin GM, Smith RNB (2000) A new boundary layer mixing scheme. Part I: scheme description and single-column model tests. Mon Weather Rev 128:3187–3199

Love BS, Matthews AJ, Lister GMS (2011) The diurnal cycle of precipitation over the Maritime Continent in a high-resolution atmospheric model. Q J R Meteorol Soc 137:934–947

Matsui T, Mocko D, Lee MI, Tao WK, Suarez MJ, Pielke RA (2010) Ten-year climatology of summertime diurnal rainfall rate over the conterminous US. Geophys Res Lett 37:L13807

Matsuno T (1966) Quasi-geostrophic motions in the equatorial area. J Meteorol Soc Jpn 44:25–43

Mcfarlane NA (1987) The effect of orographically excited gravity-wave drag on the general-circulation of the lower stratosphere and troposphere. J Atmos Sci 44:1775–1800

Moncrieff MW, Miller MJ (1976) The dynamics and simulation of tropical cumulonimbus and squall lines. Q J R Meteorol Soc 102:373–394. https://doi.org/10.1002/qj.49710243208

Moorthi S, Suarez MJ (1992) Relaxed Arakawa-Schubert—a parameterization of moist convection for general-circulation models. Mon Weather Rev 120:978–1002

Mori S et al (2004) Diurnal land-sea rainfall peak migration over Sumatera Island, Indonesian Maritime Continent, observed by TRMM satellite and intensive rawinsonde soundings. Mon Weather Rev 132:2021–2039

Nakazawa T (1988) Tropical super clusters within intraseasonal variations over the western Pacific. J Meteorol Soc Jpn 64:17–34

Neale R, Slingo J (2003) The Maritime Continent and its role in the global climate: a GCM study. J Clim 16:834–848

Ploshay JJ, Lau NC (2010) Simulation of the diurnal cycle in tropical rainfall and circulation during boreal summer with a high-resolution GCM. Mon Weather Rev 138:3434–3453

Pontoppidan M, Reuder J, Mayer S, Kolstad EW (2017) Downscaling an intense precipitation event in complex terrain: the importance of high grid resolution. Tellus A Dyn Meteorol Oceanogr 69:1–15

Prein AF, Gobiet A, Truhetz H, Keuler K, Goergen K, Teichmann C, Fox Maule C, van Meijgaard E, Déqué M, Nikulin G, Vautard R, Colette A, Kjellström E, Jacob D (2016) Precipitation in the EURO-CORDEX 0.11° and 0.44° simulations: high resolution, high benefits? Clim Dyn 46:383–412

Pu B, Dickinson RE (2014) Diurnal spatial variability of great plains summer precipitation related to the dynamics of the low-level jet. J Atmos Sci 71:1807–1817

Putman WM, Lin SH (2007) Finite-volume transport on various cubed-sphere grids. J Comput Phys 227:55–78

Rienecker MM et al (2011) MERRA: NASA's modern-era retrospective analysis for research and applications. J Clim 24:3624–3648

Rio C, Hourdin F, Grandpeix JY, Lafore JP (2009) Shifting the diurnal cycle of parameterized deep convection over land. Geophys Res Lett 36:L07809

Sato T, Miura H, Satoh M, Takayabu YN, Wang YQ (2009) Diurnal cycle of precipitation in the tropics simulated in a global cloud-resolving model. J Clim 22:4809–4826

Satoh M, Kitao Y (2013) Numerical examination of the diurnal variation of summer precipitation over southern China. Sola 9:129–133

Schiemann R, Demory ME, Mizielinski MS, Roberts MJ, Shaffrey LC, Strachan J, Vidale PL (2014) The sensitivity of the tropical circulation and Maritime Continent precipitation to climate model resolution. Clim Dyn 42:2455–2468

Schumacher C, Houze RA Jr (2003) Stratiform rain in the tropics as seen by the TRMM precipitation radar. J. Clim 16:1739–1756

Seo E, Lee MI, Kim D, Lim YK, Schubert SD, Kim KM (2019) Inter-annual variation of tropical cyclones simulated by GEOS-5 AGCM with modified convection scheme. Int J Climatol. https://doi.org/10.1002/joc.6058

Shin DW, Cocke S, Larow TE (2007) Diurnal cycle of precipitation in a climate model. J Geophys Res 112:D13109

Sorooshian S, Gao X, Hsu K, Maddox RA, Hong Y, Gupta HV, Imam B (2002) Diurnal variability of tropical rainfall retrieved from combined GOES and TRMM satellite information. J Clim 15:983–1001

Stensrud DJ (1996) Importance of low-level jets to climate: a review. J Clim 9:1698–1711

Tokioka T, Yamazaki K, Kitoh A, Ose T (1988) The equatorial 30–60day oscillation and the Arakawa-Schubert penetrative cumulus parameterization. J Meteorol Soc Japan 66:883–901

Wang B (2005) Theory. In: Lau WKM, Waliser DE (eds) Intraseasonal variability in the atmosphere–ocean climate system, 1st edn. Springer, Berlin, pp 307–360

Wang B, Chen G (2017) A general theoretical framework for understanding essential dynamics of Madden–Julian oscillation. Clim Dyn 49:2309–2328

Wang YQ, Zhou L, Hamilton K (2007) Effect of convective entrainment/detrainment on the simulation of the tropical precipitation diurnal cycle. Mon Weather Rev 135:567–585

Wheeler M, Kiladis GN (1999) Convectively coupled equatorial waves: analysis of clouds and temperature in the wavenumber-frequency domain. J Atmos Sci 56:374–399

Yang GY, Slingo J (2001) The diurnal cycle in the tropics. Mon Weather Rev 129:784–801

Yashiro H, Kajikawa Y, Miyamoto Y, Yamaura T, Yoshida R, Tomita H (2016) Resolution dependence of the diurnal cycle of precipitation simulated by a global cloud-system resolving model. Sola 12:272–276

Yuan WH, Yu RC, Zhang MH, Lin WY, Li J, Fu YF (2013) Diurnal cycle of summer precipitation over subtropical East Asia in CAM5. J Clim 26:3159–3172

Zuidema P (2003) Convective clouds over the Bay of Bengal. Mon Weather Rev 131:780–798